Multi-Nanopore Force Spectroscopy for DNA Analysis

Carolina Tropini and Andre Marziali
Department of Physics and Astronomy, University of British Columbia, Vancouver, BC, Canada V6T 1Z1

ABSTRACT   The need for low-cost DNA sequence detection in clinical applications is driving development of new techno-logies. We demonstrate a method for detection of mutations in a DNA sequence purely by electronic means, and without need for fluorescent labeling. Our method uses an array of nanopores to perform synchronized single-molecule force spectroscopy measurements over many molecules in parallel, yielding detailed information on the kinetics of hundreds of molecule disso-ciations in a single measurement.

INTRODUCTION

Applications of genomics to health care, including rapid nucleic acid-based diagnostics, will require genotyping and single nucleotide polymorphism detection technologies that are easy to use, rapid, and inexpensive. Most currently available techniques are based on real-time PCR (1) or arrayed primer extension schemes such as APEX (2,3) and are reviewed elsewhere (4). Cost and in some cases complexity continue to be a barrier to incorporation of these techniques in clinical settings. Direct detection technologies that do not require DNA modification or fluorescent labels have the potential to achieve a substantial reduction in cost, and techniques based on single molecule detection show promise in reaching levels of sensitivity and specificity appropriate for sequence detection without prior PCR amplification.

A number of groups working toward direct detection of DNA using nanopores (5–13) have demonstrated various forms of DNA analysis, primarily employing α-hemolysin (α-HL) proteinaceous pores (5,8,10,14,15). Most groups in this field aim to determine DNA sequence de novo from highly sensitive electronic or optical measurements of translocation through such pores. Instead, in recent work (5), we demonstrated the use of nanopore-based force spectroscopy to distinguish oligonucleotides of equal lengths and whose sequence differed by a single nucleotide. In this article, we propose to use an array of nanopores as a force spectroscopy (16) tool to rapidly test DNA duplexes for sequence specificity. By simultaneously performing force spectroscopy measurements on a large number of single-molecule probe-analyte duplexes, we reduced the time required to obtain statistically significant data by a factor equal to the number of pores. We show that high-quality data can be obtained in a few measurements without any loss of information compared with hundreds of consecutive single-molecule measurements.

METHODS

The method developed to perform single-molecule force spectroscopy is depicted in Fig. 1. Briefly, a probe composed of avidin-biotin-5′-poly(dA)$_{51}$(CCAAACCAACCACC-3′) is inserted in a single α-HL nanopore with its last 14 nucleotides representing the complement to an analyte sequence of interest. The probe is inserted by applying 200 mV across the pore (Fig. 1 a), effectively electrophoresing the probe into the pore. Presence or absence of the probe in the pore is detected by the amount of ionic current flowing through the pore under applied potential. The avidin anchor prevents a full translocation of the probe through the pore, leaving the 14-mer sequence to protrude on the *trans* side of the pore (Fig. 1 b). After a defined hold time to allow binding of analytes to the probe sequence, the applied voltage is decreased, leading unbound probes to exit the pore by thermal escape over the decreased electrostatic barrier (Fig. 1 c). The polarity of the voltage is then reversed to apply a force that withdraws the probe from the pore (Fig. 1 d). Analyte bound to the probe prevents it from exiting the pore under the reversed potential, as the pore is too narrow to allow translocation of the duplex strand (17). Eventually, under the applied force, which can be shown to scale linearly with the applied voltage, the duplex bonds dissociate, and the probe escapes the pore (Fig. 1 e). Dissociation times, t_{off}, which are used to estimate the characteristic dissociation time, τ_{off}, are measured for many binding events by repeating the experiment under different amounts of applied force, leading to a measure of the force-lifetime relation for the duplex.

Following Evans (16) we employ a Kramers escape model for thermal dissociation of the duplex under applied force and find the characteristic dissociation time to be

$$\tau_{off} = \tau_D e^{(E_b/k_bT)} e^{(-f/f_b)}, \qquad (1)$$

where τ_D is a diffusive relaxation time associated with the duplex, E_b is the height of the energy barrier, f is the applied force, and f_b is the thermal force scale defined as $f_b = k_bT/\Delta x$. Δx is the energy barrier width and thus related to the distance by which the molecules must be separated along the reaction coordinate for dissociation to occur.

Using this model we can extract the binding energy of the duplex and information on the width of the energy barrier that must be overcome for the analyte-probe duplex to dissociate. This information allows us to distinguish, to single-base resolution, analytes that differ from the complement of the probe sequence.

To exploit this method for rapid DNA sequence detection, measurements must be performed in parallel, and the relatively fragile organic pores should be replaced by a more robust array of synthetic pores. We envision a device consisting of arrays of thousands, or tens of thousands of nanopores in a synthetic membrane separating a chamber containing probes from a chamber containing oligonucleotides of unknown sequence. Repetitive application of the force spectroscopy method described above would lead to a determination of the presence of the probe sequences in the analyte pool.
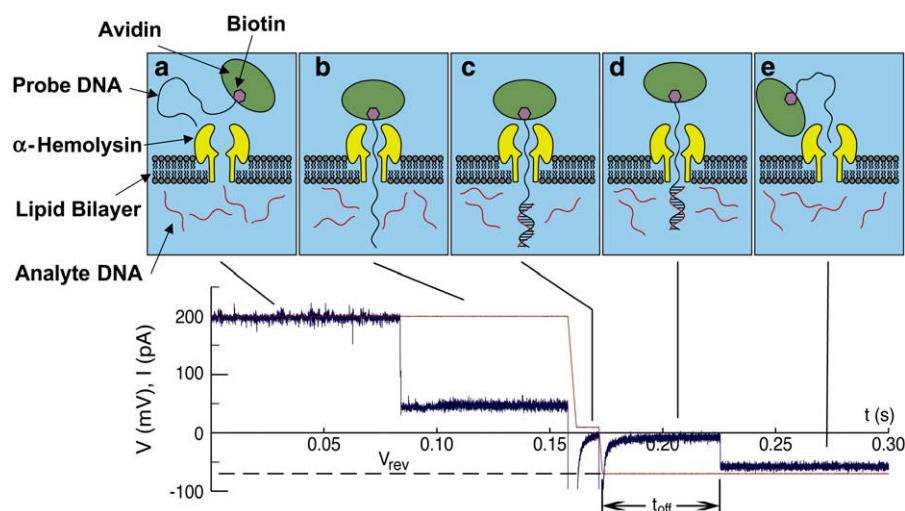
FIGURE 1 Single molecule force spectroscopy. Force is applied through electrophoretic control of a DNA homopolymer traversing a single α-HL pore and prevented from translocating by an avidin anchor. Dissociation time of a DNA duplex under force is measured for a range of applied forces. Reproduced with permission from *Biophysical Journal* (5).

Although many challenges must be overcome to produce a functioning device, we explore in this work the translation of the single-molecule measurement scheme described above to an array of many organic pores acting in parallel and synchronously. Whereas with a single nanopore, hundreds of capture-dissociation events were previously required to obtain statistically significant data, with hundreds of nanopores operating synchronously, only a few measurements are needed to achieve the same level of specificity in identifying single nucleotide mutations.

We note that though other hybridization detection methods using nanopores have been explored (10,18,19), the anchored-probe method described here allows synchronous application of force to all probe elements in an ensemble of pores. This is not possible in a multi-nanopore method employing asynchronous dissociation and translocation of probes hybridized to analyte on the *cis* side of the pore.

Using α-HL, we incorporate hundreds of pores in a single lipid bilayer and perform a protocol similar to that of Fig. 1. The signal extracted from this experiment is no longer a two-state signal, varying only in its duration in time for the single-pore experiments, but is instead a current signal that rises steadily as an increasing number of probes dissociate from analytes and exit the pore. Information on the kinetics of the dissociation and probe escape mechanisms can be extracted from this current signal.

The nanoporous membrane is assembled in vitro using a method modified from that of Akeson et al. and described in detail in previous work (5,14). Briefly, a black lipid membrane of 1,2-diphytanoyl-*sn*-glycero-3-phosphocholine (Avanti Polar Lipids, Alabaster, AL) is formed across an $\sim$50-μm hole in a Teflon tube that connects two 200-μl compartments. The reservoirs and Teflon tube are filled with microfiltered buffered 1 M KCl (10 mM HEPES, 1 mM EDTA, pH 8.0) as the conducting medium. Each reservoir contains a silver chloride-coated electrode connected to a patch-clamp amplifier (Axopatch 200B, Axon Instruments, Foster City, CA). The pores are formed by addition of monomeric α-HL (Sigma-Aldrich, St. Louis, MO) to one side of the bilayer (the *cis* side). Pore formation is detected by applying a 100-mV electric potential across the bilayer with the anode on the *trans* side of the membrane (positive and ''forward'' convention in this work) and waiting for an increase in the measured current. Under these conditions, a single open pore shows a forward conductance of $\sim$1 nS, yielding a current of $\sim$100 pA at 100 mV. When the current reaches $\sim$10–20 nA, indicating that 100–200 pores have been incorporated in the membrane, the *cis* chamber is rinsed with fresh buffer solution to prevent formation of additional pores. It is known from previous experiments that some pores will insert into the membrane in the reverse direction (with the pore vestibule on the *trans* side of the membrane) and that some pores will form hexamers or possibly other structures that may conduct current but that are not amenable to DNA translocation. Based on the similarity between the methods used here and in our previous single-channel work, we expect that the majority of

pores will be in the proper orientation and of the correct structure, though we acknowledge that some pores may conduct current while not participating in the operation of our device. Fortunately, the timescale characteristic of the current changes in the open pores is short compared with the timescales explored in analysis of the duplex dissociation. Therefore, the current from pores that do not participate in the probe capture-escape process can easily be subtracted from the measurement.

During experiments, data acquisition software and hardware (Labview, National Instruments, Austin, TX) are used to record the ionic current data and to apply controlled electric potential profiles across the pore. All data are low-pass filtered at 10 kHz and digitized at 50 kHz for analysis.

The probe molecule for the work presented in this article is constructed from a 44-mer ssDNA molecule biotinylated at its 3' end (IDT, Coralville, IA) with the 14 nucleotides at the 5' end forming the active portion of the probe (see Table 1). Probe DNA is purified by the supplier by PAGE purification. To prevent probes from translocating through the pore, avidin (Invitrogen Molecular Probes, Burlington, ON) is hybridized to the biotin to form a large molecular anchor that is excluded from the pore. The probe molecule is added to the *cis* side of the pore at a concentration of 2 μM. The analyte DNA (IDT) has no modifications. Analytes were added to the solution on the *trans* side of the pore at 10 μM before bilayer formation. Table 1 lists the sequences of probe and analyte molecules (IDT) tested in this work. The binding energies in Table 1 correspond to the calculated free energy of hybridization (20) between the analyte and the given probe. Mismatches are underlined.

Experiments with multiple pores proceed as shown in Fig. 2. Once the pores have been established (or incorporated in the membrane), and the probe and analyte molecules have been added to the *cis* and *trans* side chambers, respectively, the probe is inserted through the nanopore by application of a $+200$-mV potential across the bilayer.

TABLE 1 Probe and analyte molecule sequences, with associated hybridization energies calculated using Mfold (20), at 1.0 M KCl, 20°C

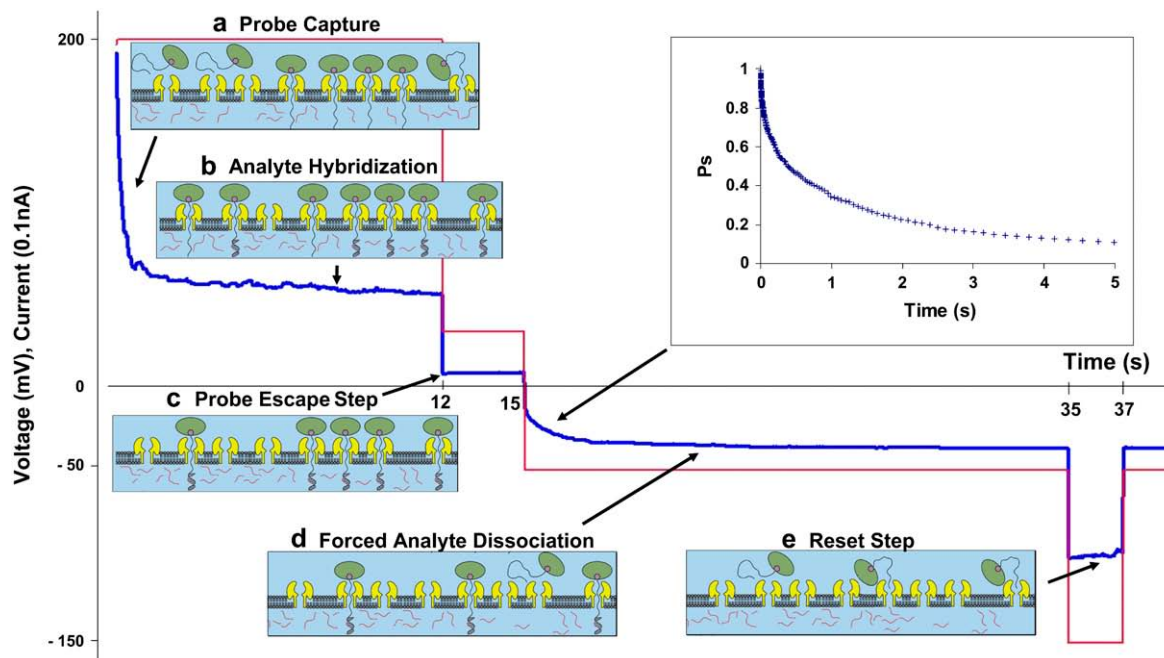| Molecule name	Sequence	ΔG (kcal/mol)
Probe	biotin-3'-(dA)$_{30}$CCAAACCAACCACC-5'	n/a
PC	5'-GGTTTGGTTGGTGG-3'	−23.1
7C	5'-GGTTTGCTTGGTGG-3'	−16.9
7T	5'-GGTTTGTTTGGTGG-3'	−17.2
10C	5'-GGTTTGGTTCGTGG-3'	−17.1
3G12G	5'-GGGTTGGTTGGGGG-3'	−17.0
PC rev	5'-GGTGGTTGGTTTGG-3'	−13.3

FIGURE 2   Force spectroscopy–based DNA analysis in multiple nanopores. (*a*) Application of capture voltage (+200 mV) leads to incorporation of probes, gradual blockage of pores, and current decrease. (*b*) Capture voltage is held while analyte binds to probes on the *trans* side of the membrane. (*c*) The voltage is decreased to 30 mV, allowing thermally activated escape of probes not bound to analyte. (*d*) Voltage is reversed to −50 mV, resulting in thermal dissociation of the analyte-probe duplex against an energy barrier that is modified by the applied potential. (*e*) Voltage is lowered to −150 mV, ensuring dissociation of any duplexes that might still be bound after *d*. The experiment is then ready to be started again. (*Inset*) Survival probability (*Ps*) as a function of time for probes bound to the PM molecule at −50 mV potential.

Fig. 2 *a* displays an exponential reduction in current to typically 20% of its initial value as an increasing number of pores are filled with probes. Control experiments without probe molecules on the *cis* side of the pores indicated steady current within ±0.5 nA (<10% of the total current) during the 12-s duration of a typical capture cycle. For typical probe concentrations of 2 μM, the characteristic time constant for probe insertion time is 0.2 s, based on an exponential fit to the current during the capture cycle (data not shown).

After 10 s, the voltage is decreased to +30 mV for 3 s, allowing probes that have not hybridized with their complement to thermally escape from the pore. Capacitive effects from the membrane are subtracted in hardware by the patch-clamp amplifier. The characteristic estimated escape time of 44-mer probes at this potential is ~1 s (data not shown). After escape of most unbound probes, the voltage is set to a negative value, applying a force tending to lower the barrier for analyte-probe dissociation and forcing escape of the analyte from the pore. After the voltage reversal, the magnitude of the current begins to increase as duplexes dissociate and probes exit the pores. Any remaining unbound probes will, under reverse potentials, escape substantially faster than probes that are bound to an analyte. In other experiments (data not shown) we find that 44-mer probes escape in <1 ms under the influence of a similar range of reverse potentials. The weakest analyte-probe combination we tested at −10 mV led to a probe escape timescale of nearly 1 s, allowing us to easily distinguish these two effects in the analysis. Furthermore, this separation of timescales supports the assumption that avidin-pore interactions play only a minor role, if any, in the dissociation measurements presented below. Similarly, pores that did not or could not receive probes during the insertion process allow current to reverse in timescales much shorter than those analyzed in our experiment. After measurement of current rise during probe-analyte dissociation, a large negative voltage reset step (Fig. 2 *e*) is applied to free any remaining probes and restore the pores to their open state. The porous membrane impedance is calculated by the analysis program before probe incorporation, at the end of

the probe incorporation, following the probe escape step, and after the reset step. Using this information, the total number of pores, number of pores filled with probe, and the number of probes with bound analyte are estimated. Estimates are based on *IV* curves (not shown) from a single pore in identical buffer conditions, which are approximated by the following relations:

Open pore:

$$V > 0: I = 0.97V; V < 0: I = 0.74V. \qquad (2)$$

Blocked pore (by probe for $V > 0$, probe and analyte for $V < 0$):

$$V > 0: I = 0.0006V^2 + 0.0953V;$$
$$V < 0: I = -0.0003V^2 + 0.0645V. \qquad (3)$$

Of the 100–200 pores formed, we find that typically 88% are filled with probe, and 75–80% of the total number of pores contain probe-analyte complexes.

Each event is analyzed by software that calculates the expected number of pores in each of the open state, the probe-captured state, and the duplex bound state and then uses the pore state information to scale each of the five events for each dissociation voltage level (or reverse voltage level) before averaging. Scaling is performed as follows to yield the survival probability of the probes in the pore:

$$P_s(t) = 1 - \frac{I(t) - I_{start}}{I_{end} - I_{start}}. \qquad (4)$$

I_{start} and I_{end} are calculated from the applied potential and from the calculated number of pores. Events are averaged after scaling, and the resulting data are sampled (by averaging over intervals) at exponentially increasing time intervals to preserve temporal resolution for short times while keeping

data files small for subsequent analysis. Only the first 90% of analyte-probe dissociations are analyzed (to $\log(P_s(t)) = -1$) to avoid the significant influence of current noise when the number of occupied pores becomes small.

A representative plot of survival probability for the perfect complement analyte at -50 mV of reverse potential is shown in Fig. 3.

RESULTS AND DISCUSSION

It was noted in the single-molecule experiments (5) that dissociation times did not follow an exponential Poisson distribution as might be expected but instead contained multiple timescales. In the previous work, a nonnegative least-squares fit over many timescales was used to extract several dominant timescales for each probability distribution, and a coefficient-weighted average of the timescales was calculated to yield a characteristic dissociation time. A more recent analysis indicated that a stretched exponential fit yielded nearly identical timescales without the need for lengthy numerical analysis, and we therefore apply it here to extract timescales for each dissociation event. We do not, however, propose a physical basis for the stretched exponential behavior, leaving exploration of the dissociation kinetics to other work in preparation. Fits shown in Fig. 3 were performed with the following model:

$$P_s(t) = A e^{-((t-t_0)/\tau_{off})^{\alpha}}. \quad (5)$$

Here α is the stretch exponent, τ_{off} is the characteristic timescale for the process, A is an amplitude coefficient to allow for small errors in the normalization (A is ~ 1 for most fits), and t_0 is a fixed small time delay of 100 μs, required for the short-time-scale fits to compensate for delay between commanded voltage reversal and actual current change. For most high-voltage ($|V| > 80$ mV) fits, $\alpha \approx 1$ and $A \approx 1$, leaving τ_{off} as the only free parameter in the fit. For lower-voltage fits, α can be as low as 0.4, showing significant deviation from exponential decay in this regime. The char-

acteristic behavior of decreasing α with diminishing reverse voltage is observed in all molecule-dissociation experiments.

The timescale of dissociation is plotted against applied force (as a potential) in Fig. 4 for each analyte molecule. For most molecules, the dissociation timescale is approximately exponential with applied force, but only at low applied force. At larger forces, the plots for all molecules converge. This behavior may be expected because the exponential relation from Eq. 1 is valid only in the regime of a significant barrier. At larger applied potentials, the energy barrier is presumably reduced substantially by the electrostatic force and eventually will vanish such that probe escape from the pore becomes a diffusive rather than a barrier-crossing process. We note that the timescale in this regime is nearing that of exit of free probes under similar potentials, observed in controls where no analyte was added to the *trans* side (data not shown). From Eq. 1, it is expected that the logarithm of the dissociation timescale in the low-voltage regime is related to the applied voltage according to

$$\ln(\tau_{off}) = \left(\frac{-zN\Delta x}{\Delta l(25mV)}\right)V + \frac{E_b}{k_bT} + \ln(\tau_D). \quad (6)$$

The electrostatic force has been approximated as $zNeV/\Delta l$, e/k_bT is $\sim (25$ mV$)^{-1}$ at 20°C, the effective charge per nucleotide is z, and N is the number of nucleotides present in the region over which the potential drop occurs (Δl). For ssDNA, $N/\Delta l = 2$ nm^{-1}, i.e., the inverse of the nucleotide spacing.

The slope of ln(dissociation time) versus potential (or force) for each molecule is expected to be proportional to the width of the energy barrier for probe escape, Δx, with steeper slope implying a wider barrier (16): at 20°C, the slope is $z\Delta x/12.5$ mV^{-1}. The reduction in barrier energy by the applied force increases with distance along the reaction coordinate, and this in turn can shift the position of the barrier's maximum. For a broad, smooth barrier, one might therefore expect the barrier width to decrease slightly with applied force, as seen in Fig. 4, particularly by the curvature in the perfect complement dissociation time under force. For more complicated barrier shapes, including possibly those of molecules containing mismatches, one might expect changes in slope to reflect the nature of the barrier shape, though extraction of such detail may be beyond the resolution of these measurements.

In any case, it is evident from Fig. 4 that dissociation times at a given potential do not necessarily follow the trend of equilibrium binding energies of the different duplexes. This is perhaps not surprising because of the inherent difference between the dissociation process followed in our experiment, where dissociation must proceed along a specific reaction coordinate, and thermal dissociation calculated using models such as Mfold (20). Even the simple barrier-crossing model employed here predicts that only the intercept of dissociation time at zero applied force is related to the binding energy.
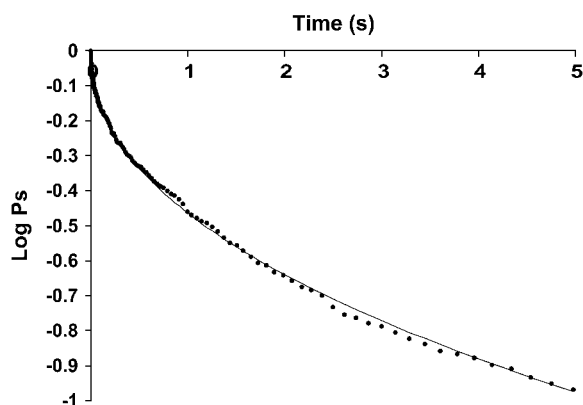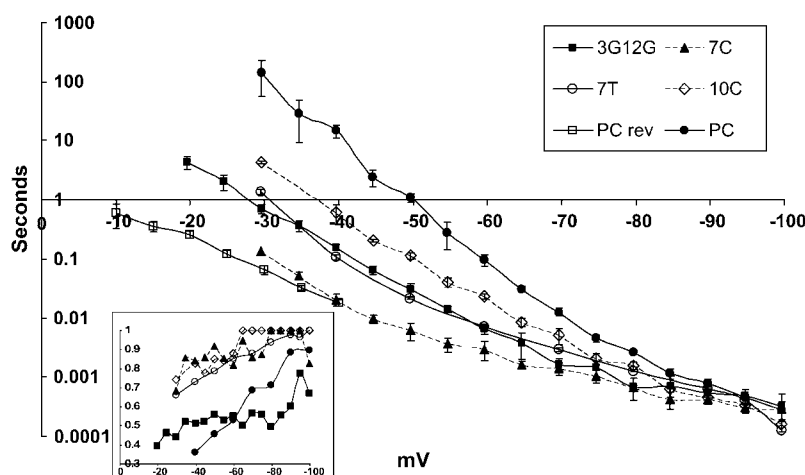

Time (s)

FIGURE 3 Scaled survival probability (*dots* represent data sampled logarithmically in time and averaged) of the perfect complement-probe duplex under -50 mV of applied reverse potential. Stretched exponential fit (*line*) yields a characteristic timescale for dissociation; here $\tau_{off} = 0.866$ s, and $\alpha = 0.46$ (see Eq. 5).

FIGURE 4 Dissociation timescale τ_{off} as a function of applied reverse potential (proportional to dissociation force, increasing to the right) for different probe-analyte combinations, including perfect complement sequence (PC), single mismatches (7C, 7T, 10C), a double mismatch sequence (3G12G), and a weakly binding reversed PC sequence (PC rev). Note that, under low applied force (-30 to -50 mV), the dissociation time for the perfect complement is over 10 times longer than any of the mismatches. At large applied forces, dissociation occurs in a regime far from thermal dissociation, and all molecule dissociations occur in similar times. The inset shows values for the stretch exponent α for each molecule versus applied potentials.

Unfortunately, because of changes in the slope for some of the molecules at the edge of the measurement regime, such an intercept can only be estimated. Fig. 5 is a plot of the estimated value of the intercept calculated from the four lowest force data points available for each molecule.

As seen in our previous work (5), a linear relation is observed between the zero-force intercept of dissociation times and duplex binding energies. The measured slope of 0.73 is similar to that measured with single-pore experiments and different from unity as expected from an Arrhenius model of dissociation. Differences between thermal dissociation and dissociation driven by force along a specific reaction coordinate may explain the deviation of the slope from the expected value. The intercept derived from Fig. 5 yields a diffusive barrier crossing attempt time (τ_{D}) of $\sim$100 ns.

These details should provide interesting avenues for further exploration of kinetics of force-driven DNA dissociation, and of DNA escape from α-HL nanopores. As a practical result, it should be noted that the dissociation time for the perfect complement at low force, for example at -40 mV, is at least 30 times greater than the dissociation time of any of the mismatches at the same voltage, implying that perfect complementarity should be relatively easy to distinguish from single or multiple mutations in a molecule.

The signal/noise ratio of our method increases with the number of pores and with the difference in ion current between open and blocked pores. Robust implementation of such a method for commercialization would therefore require synthetic membranes with a high density of pores, each with dimensions as close as possible to α-HL. To ensure high fidelity of mutation detection, and as a result of the complexity of the dissociation kinetics, an array of porous membrane elements would need to be constructed. For each single nucleotide polymorphism to be tested, there would be several porous membrane array elements, each containing a probe complementary to a specific allele.

Such a scheme, being purely electronic in nature and not requiring a labeled sample, could lead to an inexpensive, disposable device for rapid clinical detection of a significant number of polymorphisms.
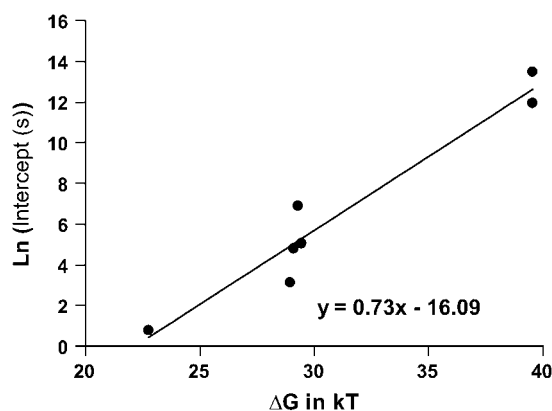
FIGURE 5 Correlation between estimated dissociation time at zero applied force and thermodynamically predicted binding energy. A slope of 1 might be expected based on an Arrhenius model of dissociation, although differences between thermal dissociation and dissociation driven by force along a specific reaction coordinate may explain the deviation of the slope from the expected value.

REFERENCES

1. Higuchi, R., C. Fockler, G. Dollinger, and R. Watson. 1993. Kinetic PCR analysis—real-time monitoring of DNA amplification reactions. *Biotechnology.* 11:1026–1030.

2. Shumaker, J. M., A. Metspalu, and C. T. Caskey. 1996. Mutation detection by solid phase primer extension. *Hum. Mutat.* 7:346–354.

3. Kurg, A., N. Tonisson, I. Georgiou, J. Shumaker, J. Tollett, and A. Metspalu. 2000. Arrayed primer extension: solid-phase four-color DNA resequencing and mutation detection technology. *Genet. Test.* 4:1–7.

4. Csako, G. 2006. Present and future of rapid and/or high-throughput methods for nucleic acid testing, *Clin. Chim. Acta.* 363:6–31.

5. Nakane, J., M. Wiggin, and A. Marziali. 2004. A nanosensor for trans-membrane capture and identification of single nucleic acid molecules. *Biophys. J.* 87:615–621.

6. Chen, P., J. J. Gu, E. Brandin, Y. R. Kim, Q. Wang, and D. Branton. 2004. Probing single DNA molecule transport using fabricated nanopores. *Nano Lett.* 4:2293–2298.

7. Deamer, D. W., and D. Branton. 2002. Characterization of nucleic acids by nanopore analysis. *Accounts Chem. Res.* 35:817–825.

8. Akeson, M., D. Branton, J. J. Kasianowicz, E. Brandin, and D. W. Deamer. 1999. Microsecond timescale discrimination among poly-cytidylic acid, polyadenylic acid, and polyuridylic acid as homopol-ymers or as segments within single RNA molecules. *Biophys. J.* 77:3227–3233.

9. Heng, J. B., A. Aksimentiev, C. Ho, P. Marks, Y. V. Grinkova, S. Sligar, K. Schulten, and G. Timp. 2006. The electromechanics of DNA in a synthetic nanopore. *Biophys. J.* 90:1098–1106.

10. Mathe, J., A. Arinstein, Y. Rabin, and A. Meller. 2006. Equilibrium and irreversible unzipping of DNA in a nanopore. *Europhys. Lett.* 73:128–134.

11. Siwy, Z., L. Trofin, P. Kohli, L. A. Baker, C. Trautmann, and C. R. Martin. 2005. Protein biosensors based on biofunctionalized conical gold nanotubes. *J. Am. Chem. Soc.* 127:5000–5001.

12. Kasianowicz, J. J. 2004. Nanopores: Flossing with DNA. *Nat. Mater.* 3:355–356.

13. Astier, Y., O. Braha, and H. Bayley. 2006. Toward single molecule DNA sequencing: Direct identification of ribonucleoside and deoxy-ribonucleoside 5′-monophosphates by using an engineered protein nanopore equipped with a molecular adapter. *J. Am. Chem. Soc.* 128:1705–1710.

14. Nakane, J., M. Akeson, and A. Marziali. 2002. Evaluation of nano-pores as candidates for electronic analyte detection. *Electrophoresis.* 23:2592–2601.

15 Vercoutere, W. A., S. Winters-Hilt, V. S. DeGuzman, D. Deamer, S. E. Ridino, J. T. Rodgers, H. E. Olsen, A. Marziali, and M. Akeson. 2003. Discrimination among individual Watson-Crick base pairs at the termini of single DNA hairpin molecules. *Nucleic Acids Res.* 31:1311–1318.

16. Evans, E. 2001. Probing the relation between force lifetime and chem-istry in single molecular bonds. *Annu. Rev. Biophys. Biomol. Struct.* 30:105–128.

17. Song, L. Z., M. R. Hobaugh, C. Shustak, S. Cheley, H. Bayley, and J. E. Gouaux. 1996. Structure of staphylococcal alpha-hemolysin, a heptameric transmembrane pore. *Science.* 274:1859–1866.

18. Kasianowicz, J. J. 2002. Nanometer, scale pores: Potential applications for analyte detection and DNA characterization. *Dis. Markers.* 18:185–191.

19. Vercoutere, W., S. Winters-Hilt, H. Olsen, D. Deamer, D. Haussler, and M. Akeson. 2001. Rapid discrimination among individual DNA hairpin molecules at single-nucleotide resolution using an ion channel. *Nat. Biotechnol.* 19:248–252.

20. Zuker, M. 2005. Mfold webserver for nucleic acid folding and hybridization prediction. *Nucleic Acids Res.* 31:3406–3415.